COMPUTER-AIDED CIVIL AND INFRASTRUCTURE ENGINEERING

Computer-Aided Civil and Infrastructure Engineering **30** (2015) 892–905

Effect of Pulse-and-Glide Strategy on Traffic Flow for a Platoon of Mixed Automated and Manually Driven Vehicles

Shengbo Eben Li*

State Key Lab of Automotive Safety and Energy, Department of Automotive Engineering, Tsinghua University, Beijing, China

Kun Deng

Department of Mechanical Science and Engineering, University of Illinois Urbana-Champaign, Urbana, IL, USA

Yang Zheng

State Key Lab of Automotive Safety and Energy, Department of Automotive Engineering, Tsinghua University Beijing, China

&

Huei Peng

Department of Mechanical Engineering, University of Michigan, Ann Arbor, MI, USA

Abstract: *The fuel consumption of ground vehicles is significantly affected by how they are driven. The fuel-optimized vehicular automation technique can improve fuel economy for the host vehicle, but their effectiveness on a platoon of vehicles is still unknown. This article studies the performance of a well-known fuel-optimized vehicle automation strategy, i.e., Pulse-and-Glide (PnG) operation, on traffic smoothness and fuel economy in a mixed traffic flow. The mixed traffic flow is assumed to be a single-lane highway on flat road consisting of both driverless and manually driven vehicles. The driverless vehicles are equipped with fuel economy-oriented automated controller using the PnG strategy. The manually driven vehicles are simulated using the Intelligent Driver Models (IDM) to mimic the average car-following behavior of human drivers in naturalistic traffics. A series of simulations are conducted with three scenarios, i.e., a single car, a car section, and a car platoon. The simulation results show that the PnG strategy can significantly improve the fuel economy of individual vehicles. For traffic flows, the fuel economy and traffic smoothness vary significantly under the PnG strategy.*

1 INTRODUCTION

Nowadays, the petroleum-based fuels generate more than 90% of the road transportation energy (Kobayashi et al., 2009). The fuel consumption of ground vehicles is affected not only by the powertrain efficiency but by how they are driven. It has been observed that driving styles can affect fuel consumption by up to 10% (Van Mierlo et al., 2004). The concept of ecological driving has attracted a lot of attention in recent years. This concept has also resulted in the changes in driver education, fuel-gauge feedback, and eco-behavior monitoring. Recent progress on vehicle automation also presents new opportunities to implement eco-driving

*To whom correspondence should be addressed. E-mail: *lisb04@gmail.com*.

DOI: 10.1111/mice.12168

technologies (Dharia and Adeli, 2003; Domínguez et al., 2013).

The eco-driving vehicles apply fuel-saving techniques to automatic control systems, e.g., adaptive cruise control (ACC), to achieve more efficient operations than human drivers, which requires good understanding of vehicle fuel consumption and load. This can be done by learning traits of fuel-efficient drivers, such as accelerating smoothly, maintaining adequate headway, eliminating excessive idling, etc. (Beusen et al., 2009; Zarkadoula et al., 2007). An alternative model-based approach is to determine fuel-saving strategies from vehicle longitudinal dynamics. Some known strategies include optimal shift-control of transmission (Setlur et al., 2003), smooth longitudinal acceleration (Li et al., 2011; Zhang and Ioannou, 2004), and traffic flow/road slope prediction (Manzie et al., 2007; Hellstrom et al., 2009). Among all strategies, the Pulse-and-Glide (PnG) strategy is known to be able to minimize fuel consumption in both free-flowing and car-following conditions (Li and Peng, 2012). This strategy uses a periodic operation, which first runs the engine at high power to accelerate, and then coasts down to a lower speed. The experiment on PnG has found that PnG can reduce fuel consumption up to 20% compared to constant speed driving. The precise mathematical solution for PnG maneuver was obtained through a constrained quasi-singular optimal control problem when a vehicle headway constraint is imposed (Li and Peng, 2012). The model-based PnG strategy is not only suitable for driver assistance but also quantitatively appealing for automated driving. The aforementioned research on the PnG strategy only studies individual vehicle behavior, and its effect on traffic smoothness and fuel consumption of traffic flow is unknown.

The impact of vehicle automation, e.g., ACC with typical following function, on traffic flow has been studied in the last decades. Most studies were based on either microscopic or macroscopic traffic simulations and focused on single lane traffic to study the issues of stability and congestion (Ioannou and Stefanovic, 2005; Kesting and Treiber, 2008). It was found that well-designed ACC can smooth out a wide class of traffic disturbances. The smooth response of ACC may also create large gaps between vehicles and invite more cut–ins from adjacent lanes, generating additional disturbances. Darbha and Rajagopal considered this issue by distinguishing two terminologies, i.e., string stability and traffic flow stability (Darbha and Rajagopal, 1999). Simulations based on macroscopic traffic flow models show that mixed traffic flow becomes unstable if the vehicles employ a constant time headway policy. This finding is consistent with some earlier studies based on microscopic models. Further study demonstrated that for ACC vehicles equipped with forward looking sensors the downstream biasing strategy could generate exponentially stable flow on a circular highway. The formation and dispersion of traffic jam is another hotspot in mixed traffic flow research. Wilson surveyed the mechanism of spatio-temporal pattern formation, including the formation and propagation of traffic jam, in highway traffic models (Wilson, 2008). In Adeli and Samant (2000), Adeli and Ghosh-Dastidar (2004), and Jiang and Adeli (2004, 2005, 2009), a mesoscopic-wavelet model was proposed for simulating freeway traffic flow patterns and extracting congestion characteristics. Davis constructed a random mixture of ACC vehicles and manually driven vehicles, and found that the formation of jams was sensitive to the sequence of vehicles and as speed increases ACC vehicles were more likely to cause congestion (Davis, 2004, 2007). Jerath and Brennan studied self-organizing traffic jams in medium-to-high density traffic flows. One observation is that while introducing more ACC vehicles can enable higher traffic flows, it also results in disproportionately higher susceptibility to congestion (Jerath and Brennan, 2010).

The objective of this article is to study the influence of fuel economy-oriented vehicle automation on a mixed traffic flow with automated and manually driven vehicles. The major contribution of this article is thoroughly analyzing a newly developed fuel-optimized driving strategy, i.e., PnG strategy, which has been proved to yield the best fuel economy for individual vehicles. Such research needs simulations using a microscopic traffic flow model in more detailed level, in particular in terms of powertrain dynamics and engine fuel consumption model. The remainder of this article is organized as follows: Section 2 reviews the fundamentals of the PnG strategy. Section 3 introduces the modeling of mixed traffic flow, including vehicle powertrain dynamics (engine fuel model is also included), human driver model, and automated controllers. Section 4 presents simulations with a single car, a car section, and a platoon, followed by analysis on fuel economy and traffic smoothness. Section 5 concludes this article.

2 FUEL OPTIMIZED DRIVING STRATEGY

2.1 Best fuel economy problem for single vehicle

Let us first discuss how to find a driving strategy in car-following scenarios for best fuel economy. This problem can be casted as an optimal control problem (OCP) over a time horizon $[0, T_f]$ (Li and Peng, 2012)

$$\min J = \int_0^{T_f} Q_s \cdot dt \tag{1}$$

where Q_s is the fuel consumption rate, T_f is the final time. The optimal control problem should satisfy a set of equality constraints and inequality constraints, listed as follows:

$$\frac{i_g i_0 \eta_T}{r_w} T_e = M\dot{v} + C_A v^2 + Mgf$$

$$T_{e\min} \le T_e \le T_{e\max}$$
$$\omega_{e\min} \le \omega_e \le \omega_{e\max}$$

where v is the vehicle speed, M is the vehicle mass, i_g is the speed ratio of automatic transmission, i_0 is the speed ratio of final gear, T_e is the engine torque, η_T is the mechanical efficiency of the driveline, r_w is the wheel radius, C_A is the coefficient of aerodynamic drag, g is the constant of gravity, f is the coefficient of rolling resistance, ω_e is the engine speed, $T_{e\min}$ and $T_{e\max}$ are the bounds of engine torque, $\omega_{e\min}$ and $\omega_{e\max}$ are the bounds of engine speed. Here, we impose additional inequality constraints on inter-vehicle distance to fulfill the car-following function

$$\xi_{\min} \le d - d_{des} \le \xi_{\max} \tag{2}$$

where d is the distance between vehicles, d_{des} is the desired distance set by the driver or the automated controller, and $\xi_{\min}, \xi_{\max}$ are the allowable bounds for the distance error between d and d_{des}.

2.2 Pulse-and-Glide strategy

The numerical solution of abovementioned OCP is found to take the form of a PnG strategy in car-following conditions for medium vehicle speed, and constant speed driving for speed higher than a threshold. The PnG driving strategy uses a periodic operation, which first runs the engine at high power to accelerate, and then coasts down to a lower speed. Theoretical analysis points out that the optimal solution is governed by the nonlinear static fuel consumption of internal combustion engine, which is a function of first concave up and then concave down with respect to power demand.

The concept of PnG operation is illustrated in Figure 1a, summarized as below:

Property 1: The engine switches between its minimum BSFC (Brake Specific Fuel Consumption) point and the idling point, periodically undergoing two phases, i.e., pulse and glide.

Property 2: The inter-vehicle distance oscillates between its upper and lower bounds, and the average speed of the following car is equal to that of the leading vehicle.

Property 3: The inter-vehicle distance reaches its bounds when two successive cars have identical speeds.

Figure 1b illustrates the fuel-saving mechanism of the PnG operation. The PnG operation periodically

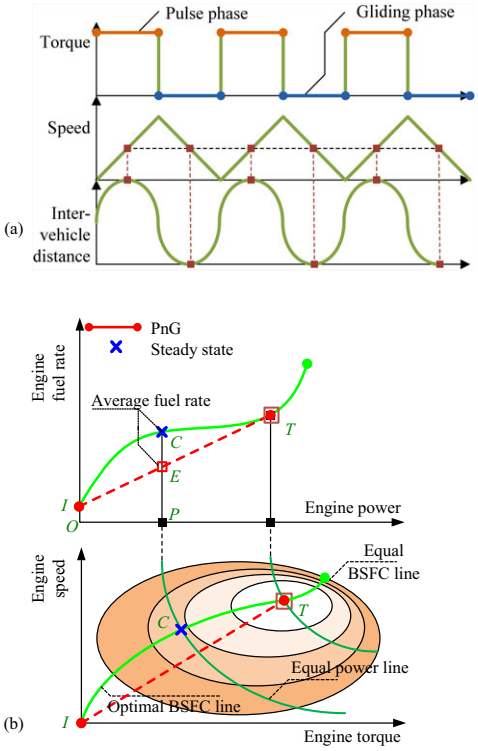

Fig. 1. Concept of PnG driving strategy (Point I - idling point; Point T- minimum BSFC point): (a) Torque, speed, and distance profiles of PnG operation, (b) the fuel-saving mechanism of PnG.

switches engine operating points between idling point (Point I) and minimum BSFC point (Point T), while any steady state operation runs engine at a fixed point, e.g., Point C. In Figure 1b, the upper side shows the engine fuel rate with respect to the engine power, and the lower side shows the engine BSFC contour. The internal combustion engine, either gasoline or diesel, has a special fueling feature, which has a minimum BSFC point (i.e., Point T here), and enlarges fuel consumption as going away. Such a feature leads to the S-shaped nonlinearity of the fuel rate for optimal BSFC line (see Figure 1b). Under the same engine power demand, the steady state operating strategy allows the engine to work on Point C, while the PnG operation switches between two points with lower average fuel rate at Point E. This shows why the PnG operation has better fuel economy.

3 MIXED TRAFFICF LOW MODEL IN SINGLE LANE

3.1 Model configuration of mixed traffic flow

The vehicle platoon runs on a straight and flat highway. The platoon is mixed, containing both manually driven

and automated vehicles with randomly selected initial states. All vehicles are assumed to be passenger cars equipped with internal combustion engine (ICE) and continuous variable transmission (CVT). They are only different by the ways they are driven: human drivers (HD) are used for manually driven cars and longitudinal automated controllers are used for driverless cars. Here, a detailed nonlinear model of vehicle longitudinal dynamics is described to capture the powertrain dynamics accurately. The constant time headway (CTH) policy, frequently adopted for desired inter-vehicle distance for automated vehicles, is also used in this article.

3.2 Model for vehicle longitudinal dynamics

The longitudinal vehicle dynamics are given by

$$\begin{aligned} \dot{v} &= \frac{i_g i_0 \eta_T}{M r_w} T_e - \frac{1}{M r_w} T_b - \frac{1}{M}\left(C_A v^2 + Mgf\right) \\ T_e &= \mathrm{MAP}\left(\omega_e, \alpha_{thr}\right) \\ T_b &= \frac{K_b}{\tau_b s + 1} P_{brk} \end{aligned} \tag{3}$$

where MAP(n) is the tabular function of engine torque, ω_e is engine speed, α_{thr} is the throttle angle, T_b is the brake torque, and P_{brk} is the brake pressure, K_b is the braking gain, and τ_b is the time constant of braking dynamics. Interested readers can refer to Li and Peng (2012) and Li et al. (2012) for more details. In hybrid vehicle design studies, static fuel maps are commonly used to predict fuel consumption. The transient behaviors of internal combustion engine reduces the torque by about 4∼5% due to effects such as inhomogeneous air/fuel mixture and incomplete combustion. A recent experimental study shows that for a heavy-duty diesel engine, the accumulated error of a static fuel model is about 4% for a European Transient Cycle. To capture its effect on fuel consumption, we add a correction term to engine static fuel consumption

$$Q_s = q_s\left(T_e, \omega_e\right) + k_e \cdot \mathrm{sat}\left(\frac{dT_e}{dt}\right)^2 \tag{4}$$

where Q_s is total fueling rate, q_s is the static fueling rate, which is the function of T_e and ω_e, k_e is a correction coefficient, and sat(n) is the saturation function. The correction coefficient is selected to increase the static fuel consumption by 4% under the FTP-72 driving cycle.

3.3 Model for human drivers

In this research, the design of fuel consumption model and microscopic traffic flow model are separated. This is mainly because of the used PnG strategy, which takes engine torque as the control input. This separation actually matches with the fact that microscopic operating behaviors of drivers are generally assumed to be decoupled with powertrain dynamics. Except for structural conciseness, the selection of miscroscopic traffic flow model needs to consider its accuracy to capture driver car-following dynamics in both micro- and macroscopic levels. A number of microscopic car-following models have been introduced so far (Ghosh-Dastidar and Adeli, 2006; Castillo et al., 2014; Ngoduy and Wilson, 2014; Ward and Wilson, 2011). The human driver model used here is an improved version of the Gipps model, called the Intelligent Driver Model (IDM) (Treiber et al., 2000; Helbing et al., 2009). The IDM model has crash-free collective dynamics, exhibits controllable stability properties, and has only six meaningful parameters, which can be easily calibrated using real-world traffic data. This model is known to provide accurate imitation for traffic flow and major traffic physical patterns but not necessarily to provide instantaneous accurate estimation for speed and acceleration. Kesting et al. (2010) has implemented IDM as an adaptive cruise control strategy with smooth transitions between acceleration and deceleration behavior, demonstrating good mimic of driver operations. The IDM model is

$$a_{des} = a_0\left[1 - \left(\frac{v}{v_0}\right)^{\delta} - \left(\frac{d_{des}\left(v, \Delta v\right)}{d}\right)^2\right] \tag{5}$$

where a_{des} is the desired acceleration, a_0 is the comfortable acceleration, δ is the acceleration exponent, v_0 is the desired speed in free traffic. The desired distance d_{des} is defined as

$$d_{des} = d_0 + \max\left(0, v\tau_h + \frac{v \cdot \Delta v}{\sqrt{4 a_0 b_0}}\right) \tag{6}$$

where τ_h is the desired time headway, b_0 is the comfortable deceleration, Δv is the relative speed to the front vehicle, d_0 is the minimum gap at stopping. The parameters of the IDM model are listed in Table 1. The stability of car-following models is an important concern for traffic simulation. Ward and Wilson (2011) first

Table 1
Parameters for the IDM model (Helbing et al., 2009)

Parameter	*Description*	*Value*
v_0	Desired speed	33.3 m/s
τ_h	Time headway	1.5 s
d_0	Minimum gap	2 m
δ	Acceleration exponent	4
a_0	Comfortable acceleration	1 m/s^2
b_0	Comfortable deceleration	3 m/s^2

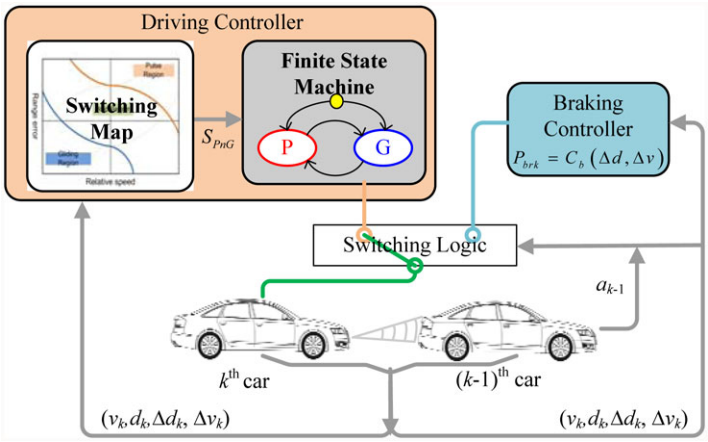

Fig. 2. Switching-based control framework for the PnG Algorithm.

presented the mathematical criteria that distinguish between convective string instability and absolute string instability. The chief idea is to calculate ranges of wave speeds that correspond to the propagation of information in the frame of the road. By selecting different parameters, IDM can exhibit stable, meta-stable, or unstable behaviors. The IDM model under the parameters in Table 1 is platoon stable, but shows no string-stable behavior, which is unfavorable to traffic fuel efficiency.

The output from the IDM model is desired acceleration, which needs to be further processed to obtain the engine/brake commands. The commands are calculated using a static inverse of the vehicle longitudinal dynamics

$$\begin{cases} \alpha_{thr} = \text{MAP}^{-1}\left(\frac{r_w}{i_g i_0 \eta_T}\Delta F, \omega_e\right) \\ P_{brk} = 0; \end{cases}, \text{if} \quad a_{des} > a_{thresh} \tag{7}$$

$$\begin{cases} \alpha_{thr} = 0 \\ P_{brk} = \frac{r_w}{i_g i_0 \eta_T K_b}\Delta F \end{cases}, \text{if} \quad a_{des} \le a_{thresh} \tag{8}$$

where a_{thresh} is the threshold of acceleration between driving control and braking control, $\text{MAP}^{-1}(n)$ is the inverse function of MAP(·), and ΔF is the force demand on wheels from external resistances, defined as

$$\Delta F = C_A v^2 + Mgf - Ma_{des} \tag{9}$$

The switching structure is used to avoid simultaneously applying both driving and braking (Li et al., 2011). The parameter a_{thresh} is a function of vehicle speed and calculated from coast-down tests with neutral gear condition. A hysteresis layer is often added to avoid frequent switching.

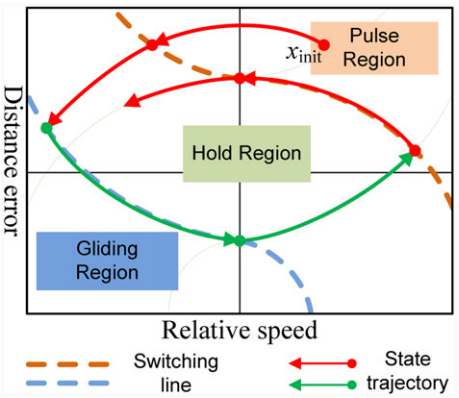

Fig. 3. The three regions of the PnG switching map.

3.4 Controller for automated vehicles

The automated controller is designed based on PnG strategy to minimize fuel consumption. A switching-based control framework is proposed for the real-time implementation, shown in Figure 2. It contains a driving controller, a braking controller, and a switching logic. The driving controller is based on the PnG strategy. It also has a switching structure, including a switching map and a finite state machine. The switching happens between two modes, i.e., pulse (P) and glide (G). In the P mode, the engine runs at the minimum BSFC point, with $T_e = T_{eBSFC}$ (engine torque at mínimum BSFC point). In the G mode, the engine is idling with $T_e = 0$ (the idling torque is zero). The switching signal S_{PnG} drives the finite state machine

$$\text{Mode}(n) = \begin{cases} \text{P} & \text{if} \quad S_{PnG}(n) = 1 \\ \text{G} & \text{if} \quad S_{PnG}(n) = -1 \end{cases} \tag{10}$$

where n is the current control step. The switching map is shown in Figure 3, where the x-axis is the relative

speed (Δv) and the y-axis is the distance error ($\Delta d = d - d_{des}$). It has two switching lines (upper and lower), which are the state trajectories when $T_e = T_{eBSFC}$ (P mode) and $T_e = 0$ (G mode), respectively. The map is then divided by two switching lines into three regions: Pulse region, Hold region, and Glide region.

The finite state machine is used to execute the transition between P and G modes. The key is how to drive the state into the hold region. In the P mode, any state (x_{init}), starting from the pulse region, will move leftwards, cross the hold region, and enter the gliding region; if we switch to the G mode at the lower switching line, the state will then move rightwards and return to the hold region. By alternating between the P and G modes, we achieve the pulse and glide operation. The switching logic is expressed as

$$S_{PnG}(n) = \begin{cases} 1 & \text{if} \quad x \in \text{PulseRegion} \\ S_{PnG}(n-1) & \text{if} \quad x \in \text{HoldRegion} \\ -1 & \text{if} \quad x \in \text{GlidingRegion} \end{cases} \tag{11}$$

$$x(n) = \begin{bmatrix} \Delta v(n) \\ \Delta d(n) \end{bmatrix}$$

Such a switching logic drives the state in the counterclockwise direction around the acorn-shaped loop. In engineering practice, some modifications are needed additionally to handle three practical issues, i.e., (1) vehicle speed fluctuates periodically and somewhat increases the load; (2) the powertrain dynamics is unmodelled, which delays the action of engine power when switching to next mode; (3) the frontal traffic flow is dynamic, not constant, which decreases the ability of holding distance constraint. A compensator is used to compensate for the effects of first two issues and a predictor is used to predict the speed of leading vehicle to avoid the violation of distance constraint. Interested readers can refer to Li et al. (2012). The PnG controller does not apply brake and thus has limited decelerating ability. It is necessary to include a braking controller for safety consideration, but its use will hurt fuel economy. Braking is a major cause of lower fuel economy in highly dynamic traffic conditions.

4 SIMULATION AND ANALYSIS

The traffic flow model is implemented in Matlab/Simulink. Three types of simulations are performed here, i.e., simulation with a single car, with a car section, and with a platoon of cars. The simulation configurations are depicted in Figure 4. The "car section" defines a section of cars with the leader being an automated car, followed by a number of manually driven cars. The section is called "mixed" if the leader is an automated car; it is called "normal" if the leader is a manually driven car. One key parameter for a car section is the sectional length, defined as the total number of cars. A platoon, either mixed or normal, is composed of sections with different sectional lengths. The behavior of mixed sections plays an important role in determining the characteristics of a mixed platoon.

Before presenting the simulation results, we define two indices to measure the characteristics of a platoon, i.e., traffic smoothness and fuel economy. The traffic smoothness is measured by the acceleration noise (shorted as AN) proposed by Helbing, Treiber, Kesting, et al. For a single car, the AN is the standard deviation of longitudinal acceleration in m/s^2. For a section or a platoon, AN is the average value of all vehicles, i.e.,

$$\text{AN} = \frac{1}{N}\sum_{k=1}^{N} std\left(a_k(t)\right) \tag{12}$$

where N is the number of vehicles in a section or a platoon. To measure the fuel economy, we use the Fuel consumption Per Hundred Kilometers (shorted as FPHK) in L/100km

$$\text{FPHK} = \frac{1}{N}\sum_{k=1}^{N} \frac{\int_0^T Q_{s,k}(t)dt}{\max\left(\varepsilon, \int_0^T v_k(t)dt\right)} \tag{13}$$

where T is the simulation duration, and $\varepsilon > 0$ is a rather small number to avoid the singularity of the denominator. The definition of FPHK is applicable for a single car, a section, or a platoon.

4.1 Simulations with a single car

In the simulations, the following vehicle (FV) is controlled either by the automated controller or a human driver. The lead vehicle (LV) is designed to follow different speed profiles. Three speed profiles are considered: (1) cut-out scenario; (2) constant speed; (3) actual driving data from naturalistic traffic flow.

4.1.1 Cut-out scenario. In the cut-out scenario, the initial speed of LV is 15 m/s which jumps to 20 m/s at 50 seconds. Meanwhile, the inter-vehicle distance increases by 10 m. Figure 5 shows the simulation results and Figure 6 compares the engine operating points. As shown in Figure 5, with the PnG strategy, the throttle angle switches between 45% (engine minimum BSFC point) and 5% (engine idling point). The headway oscillates between its upper and lower bounds ($\xi_{max} = 3$ m). With the human driver, the engine torque gradually converges to a steady state. The fuel economy of the PnG strategy is significantly improved compared to the normal human driver.

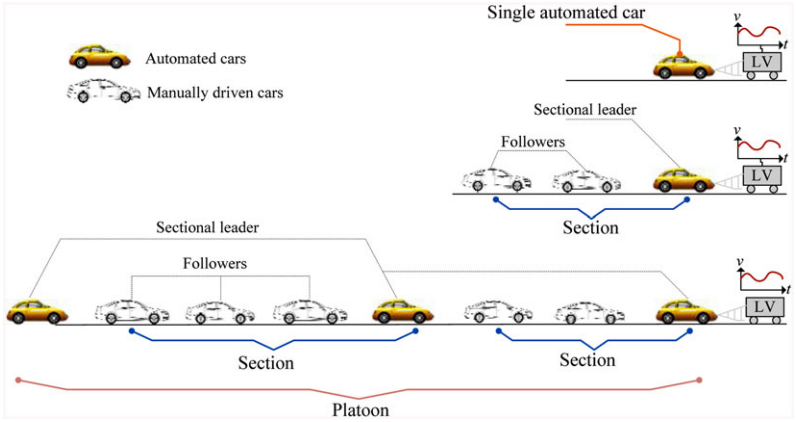

Fig. 4. Simulation configurations for mixed traffic flow (top: a single car; middle: a car section; bottom: a platoon).

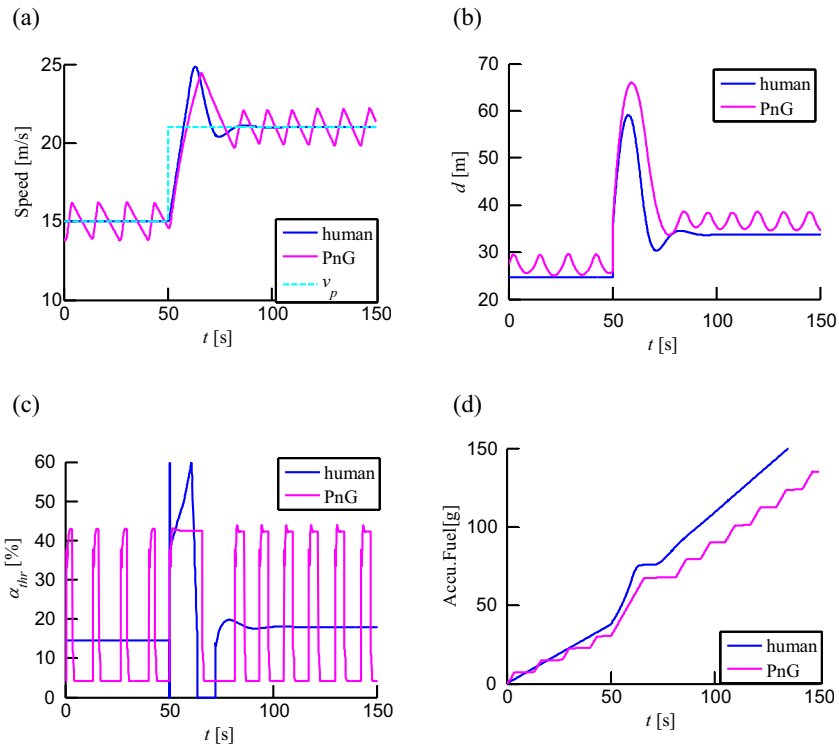

Fig. 5. Simulation results with a step change in the lead vehicle speed: (a) vehicle speed, (b) inter-vehicle distance, (c) throttle angle, (d) accumulative fuel.

4.1.2 Constant speed driving scenario. In this scenario, the LV runs at different constant speeds, ranging from 5 m/s to 35 m/s. Figure 7 compares the acceleration error and fuel consumption of FV. Again the human driver has smooth throttle command, leading to much lower acceleration noise. In addition, the acceleration noise in PnG decreases as the vehicle speed increases. Two reasons are the longer PnG period and less frequent oscillation at high speeds. The fuel economy of PnG exhibits a valley shape with lower fuel consumption in the middle speed region and higher fuel consumption on both ends. At low speeds, more frequent oscillations increase engine transient operations, which incur more fuel consumption. At very high speeds, the required power becomes higher than what the minimum BSFC points can provide. The switching operation disappears and no fuel-saving is possible.

4.1.3 Naturalistic traffic flow. The fuel economy benefit of PnG not only depends on vehicle speed, but also

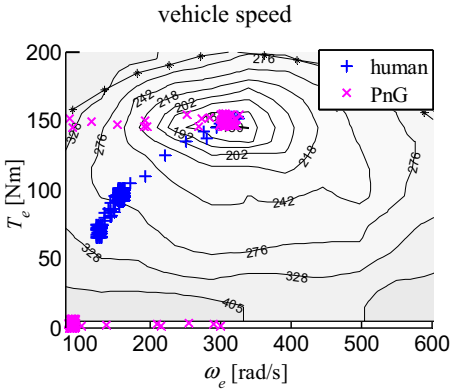

Fig. 6. Engine operating points with a step change in the lead vehicle speed (Contour-engine BSFC line).

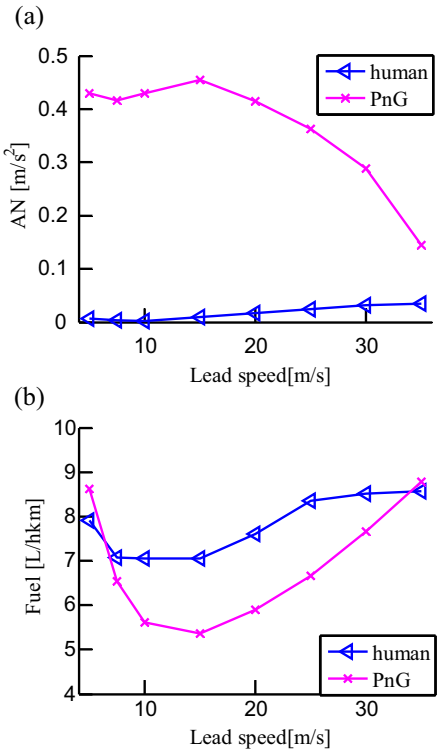

Fig. 7. Simulation results in constant speed scenarios: (a) acceleration noise, (b) fuel consumption.

depends on how dynamic the LV is. In this simulation, the baseline speed profile of LV comes from experimental data in and around Beijing (Figure 8), but scaled up or down to have different average speed (from 6 m/s to 30 m/s), and scaled in the time domain to have different acceleration level (from 0 m/s^2 to 3.5 m/s^2 in standard derivation of acceleration). Figure 9 summarizes the acceleration noise and fuel economy of the FV in the conditions of different LV speed and acceleration.

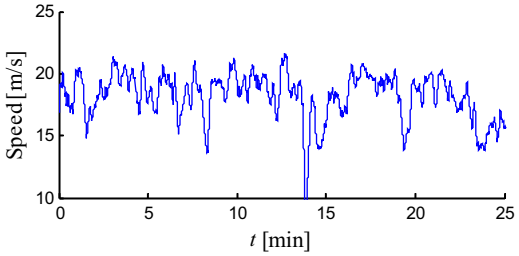

Fig. 8. Baseline speed profile from naturalistic traffic flow.

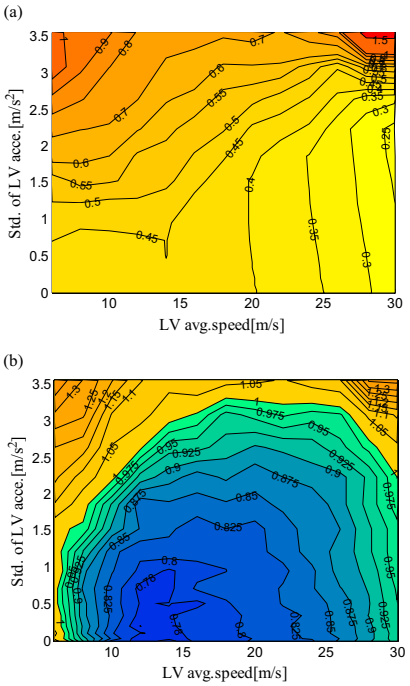

Fig. 9. Performance comparsion in different conditions: (a) increase in AN (PnG vs. human), (b) fuel consumption ratio (PnG/human).

As shown in Figure 9, the AN of PnG is higher than that of human driver, with difference between 0.25 m/s^2 and 1.5 m/s^2. The fuel-saving region of PnG is like a shell shape. The maximum fuel benefit happens when the LV speed is around 13 m/s (no acceleration). When the LV begins to oscillate in speed, the fuel economy reduces and eventually vanishes completely.

4.2 Simulations with a car section

In the following, we first define three patterns of car sections according to their fuel economy behavior. Then, we study two key factors, i.e., speed and acceleration of LV, and specify the forming region of each pattern. The superposition effect of sections is then discussed to see how sectional behavior affects the features of a platoon.

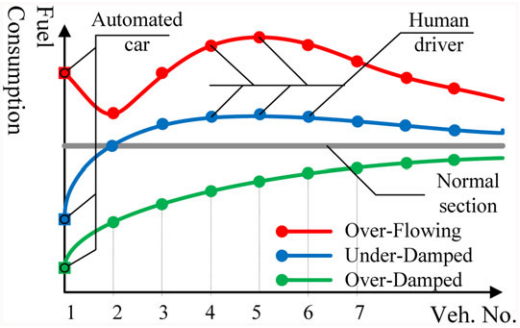

Fig. 10. Concept of three sectional patterns.

4.2.1 Analysis of sectional patterns. In a mixed section, the leader is an automated car, followed by a number of manually driven cars. The fuel benefit of the automated car depends on LV speed and LV acceleration. The behavior of a mixed section can be categozied into three patterns according to the evoluation of fuel consumption in the car section, i.e., over-flowing (OF) pattern, under-damped (UD) pattern, and over-damped (OD) pattern. The concept of these three patterns are illustrated in Figure 10.

In a car section, if the leader consumes more fuel than a manually controlled vehicle, all its followers will inheritate this "fuel-wasting" property, leading to a fuel-wasting section compared to a normal section. This behavior is called the OF pattern. In addition, there exists a V-shape in the low vehicle number. This is the joint-operation result of the PnG strategy and smoothing strategy. The first follower helps reduce the fuel consumption because of the smoothing function of human drivers. This reduces the strength and number of brakes. As the vehicle number increases, engine operating point will be distorted far from the minimum BSFC point, which increases the fuel consumption. If the leader possesses a fuel-saving property, there are two possibilities for the followers. One possibility is that all followers will be fuel saving, but the benefit reduces gradually and eventually drops to that of a normal section (all cars are driven by human drivers). This is called an OD pattern. The other possibility is that the closest followers may still be fuel-saving, but fuel consumption becomes higher than a normal section in downstream, and eventually converges back to that of a normal section. This is called a UD pattern. It is observed from simulations that the formation of sectional patterns depends on how the LV behaves in both speed and acceleration. Figures 11–13 illustrate the occurance of three patterns. In both the OF and OD patterns, the manually driven vehicles have similar behavior to the leading automated vehicle. This behavioral similarity gradually decreases downstream, dropping to the level

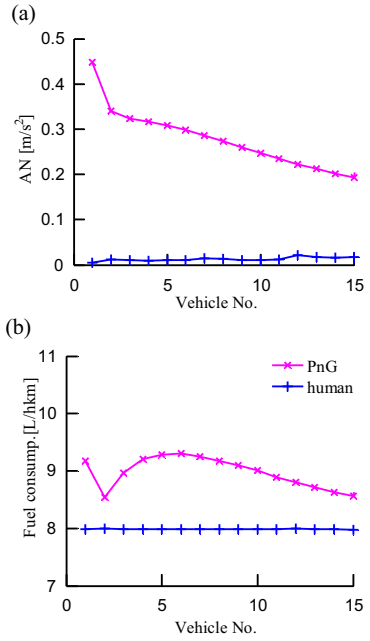

Fig. 11. Over-flowing (OF) pattern (N = 15, LV speed = 5 m/s) (a) acceleration noise, (b) fuel economy.

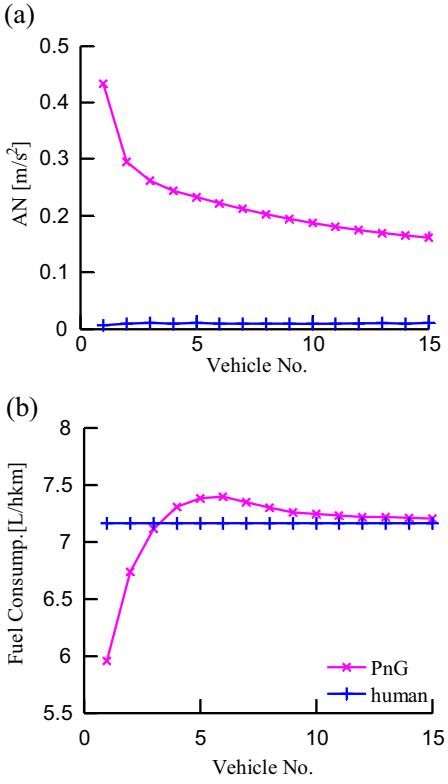

Fig. 12. Under-damped (UD) pattern (N = 15, LV speed = 10 m/s): (a) acceleration noise, (b) fuel economy.

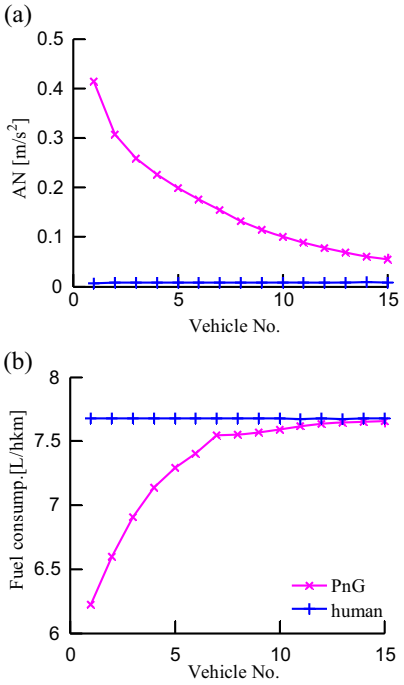

Fig. 13. Over-damped (OD) pattern (N = 15, LV speed = 20 m/s): (a) acceleration noise, (b) fuel economy.

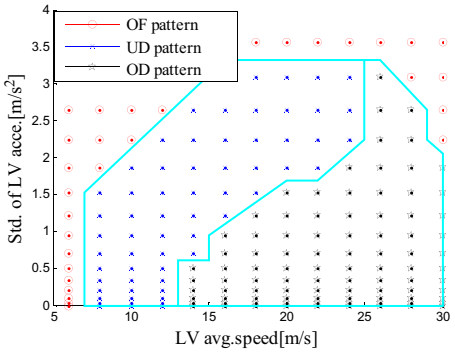

Fig. 14. Regions of section patterns.

of a normal section. In the UD pattern, the behavioral similarity does not exist.

4.2.2 Sectional pattern formation and performance. In the following, we discuss the formation of sectional pattern and its effect on the overall fuel economy. The sectional patterns mainly depend on how the LV behaves in both speed and acceleration. A number of simulations with both mixed sections and normal sections have been conducted, with LV acceleration noise ranging from 0 m/s^2 to 3.5 m/s^2 and LV average speed ranging from 5 m/s to 30 m/s. The sectional pattern is summarized in Figure 14. The blue lines are boundaries of the three patterns. From Figure 14, it is observed that

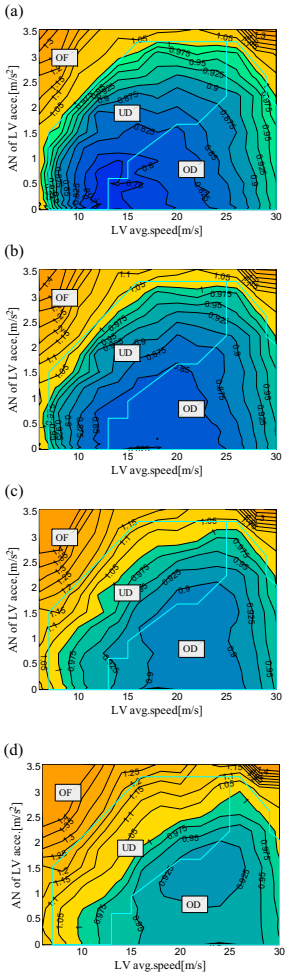

Fig. 15. Evolution of section patterns as the section length increases: (a) length = 1, (b) length = 2, (c) length = 5, (d) length = 11.

the OF pattern always accompanies a leader with fuel-wasting property. The fuel-saving region in Figure 14 is shared by two other patterns, i.e., UD and OD.

The above analysis reveals two facts: (a) a section with OF pattern always wastes fuel and (b) a section with OD pattern always saves fuel. The section with UD pattern is more complex because vehicles gradually change from fuel-saving to fuel-wasting. The section length is a critical factor that affects the average fuel consumption. Figure 15 shows the sectional fuel economy as the length increases from $N = 1$ to 11. It is observed from Figure 15 that when the sectional length is 1, both OD and UD pattern saves fuel. As the sectional length increases, the fuel-saving region in UD pattern gradually shrinks. The fuel-saving feature maintains in OD pattern, but fuel benefit becomes less. It is apparent that the point with maximum fuel benefit moves rightwards as the sectional length increases.

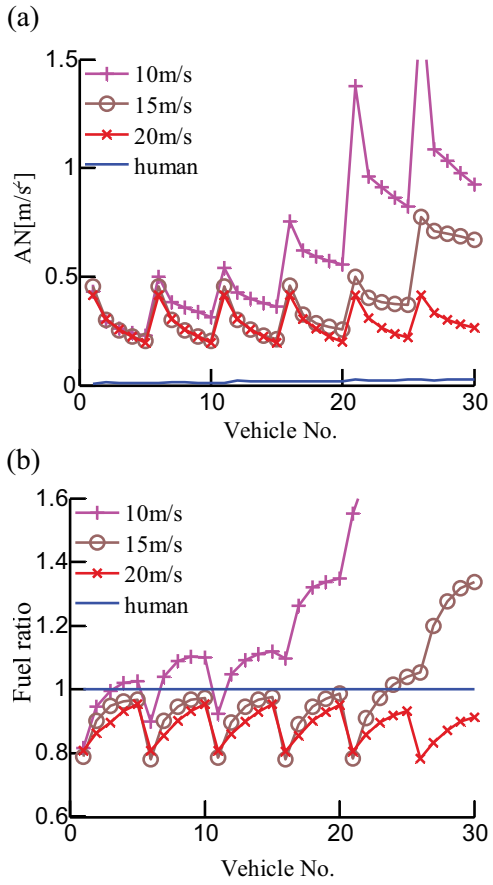

Fig. 16. Superpostion effect of sections (section number = 6): (a) acceleration noise, (b) fuel ratio.

Meanwhile the value of fuel benefit also drops. When the sectional number increases from $N = 1$ to 11, the fuel benefit of PnG compared with human drivers reduces from 24% to 10%.

4.2.3 Superposition effect of multiple sections. A car platoon can include several sections. Even when each section is fuel-saving individually, it is not clear that the resulting platoon will always be fuel-saving. The major reason is the accumulation of acceleration noise, which increases the disturbance of the following sections. If some sections are not well designed, the downstream section may face higher acceleration and eventually leads to fuel-wasting traffic.

Figure 16 illustrates examples of the superposition effect. It is shown that the OF sections always lead to fuel-wasting platoon. For sections that have UD and OD patterns, their fuel-saving behavior depends on platoon length. Fuel-saving is possible if acceleration noise does not amplify along the platoon. The performance is especially poor at low vehicle speed (5 m/s and 10 m/s).

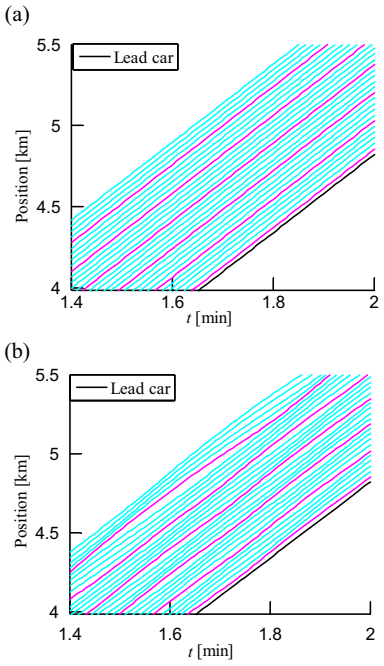

Fig. 17. Time-position (T-P) diagram (LV speed = 20 m/s, 6 auto cars): (a) human driver, (b) automated vehicle.

This may not be a concern as the ideas of PnG operation originated from middle/high-speed driving. When the vehicle speed is low, naturally we should not apply PnG anyway. So even if the analysis results show deteriorated performance, it is not a concern in practice.

4.3 Simulations with a platoon

The simulation with a platoon is designed to have 30 cars. There are two simulation scenarios: one is mixed with automated cars and the other is purely manually driven. In the first scenario, the number of automated cars is chosen as 2, 4, 6, 8, 10, 12, which represents penetration rates of 6%, 13%, 20%, 26%, 33%, and 40%. The LV of the platoon is chosen to run at constant speed 5 m/s, 10 m/s, 15 m/s, 20 m/s, 25 m/s, 30 m/s, and 35 m/s, respectively. The first car after LV is always an automated car. All other automated cars distribute uniformly. In the second scenario, all vehicles are manually driven and all the parameters are identical to the first scenario.

4.3.1 Fundamental diagram of mixed traffic. Figure 17 demonstrates the major differences of two scenarios using the time-position diagram. In Figure 17, the automated car number is set to be 6 and the LV speed is set to be 20 m/s. The pink lines in Figure 17b represent automated cars. Figure 18 is the corresponding

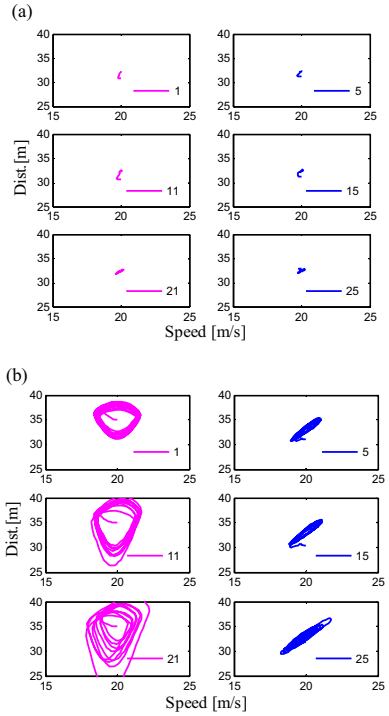

Fig. 18. Velocity-distance (V-D) diagram (LV speed = 20 m/s, car no. = 1st, 5th, 11th, 15th, 21st, 25th): (a) human driver, (b) automated car.

velocity-distance phase plot of selected cars. It is apparent that manually driven cars run homogeneously in both the spatial and temporal domains. In mixed traffic flow, however, automated car oscillates in both speed and distance to gain fuel benefit. The oscillation amplifies toward the end of the platoon, which deteriorates traffic smoothness.

4.3.2 Overall performance comparison. Figure 19 illustrates their influences on traffic smoothness and fuel economy, respectively under uniform LV speed. Different lines represent different market penetration of driverless cars, ranging from 6% to 40%. With increasing LV speed, traffic smoothness improves. This is due to the characteristic of a PnG controller, which reduces fluctuating period at high speed. The higher penetration leads to higher acceleration noise. The general influence on fuel consumption resembles the shape of a fishhook with respect to LV speed. The PnG strategy is not fuel efficient at low vehicle speed because: (1) smaller or even disappeared fuel-saving using PnG strategy, as shown in Figure 7; (2) increased use of friction brake; and (3) the accumulation of acceleration fluctuation, which in turn deteriorates fuel economy.

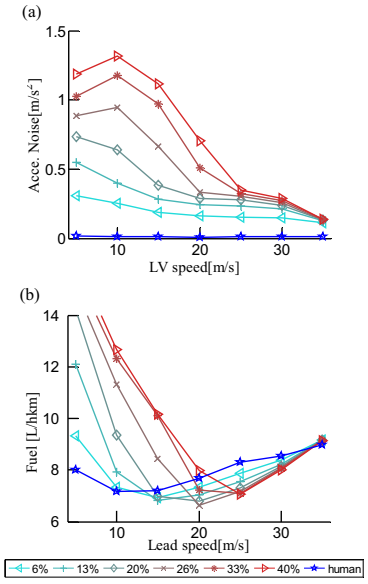

Fig. 19. Performance comparison at different penetration levels of automated cars: (a) acceleration noise, (b) fuel economy.

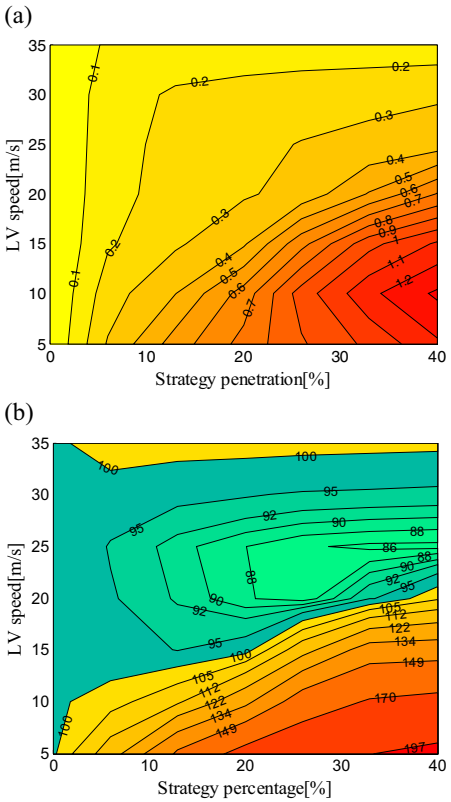

Fig. 20. Performance comparison of mixed platoon: (a) difference of AN [m/s2] (error = PnG-human), (b) fuel ratio [%] (ratio = PnG/human).

Figure 20 shows the influence of two key factors on fuel economy. The fuel-saving region is highlighted by cool color and the fuel-wasting region is highlighted by warm color. The fuel-saving region is limited to a specific range of LV speed, which becomes narrower as the market penetration increases. The maximum fuel benefit occurs at around 25 m/s and the benefit first improves with the penetration, but then reduces. The maximum improvement occurs at more than 30% penetration. Higher penetration, however, also increases the acceleration noise, which decreases the smoothness of traffic flow.

5 CONCLUSIONS

This article studies the performance of PnG operation, a fuel optimizing strategy on mixed traffic flow, especially in terms of traffic smoothness and fuel economy. The research relies on a microscopic traffic flow model, which contains both automated cars and manually driven cars. Numerical simulations are conducted for individual car, car section, and platoon scenarios, respectively. The major findings include:

1. The PnG controller has an oscillating behavior and its acceleration noise is higher than that of human drivers. The engine switches between its minimum BSFC point and the idling point, periodically undergoing two phases, i.e., pulse and glide. Compared to steady cruising, the fuel economy of PnG exhibits a valley shape with better fuel economy in the middle speed region and worse fuel economy on both ends.
2. A mixed car section has three patterns of behavior, i.e., OF, UD, and OD. The behavior patterns depend on the speed and acceleration of the lead vehicle. The section with OF pattern always wastes fuel; the section with OD pattern always saves fuel; for a section with UD pattern, cars can change from fuel-saving to fuel-wasting downstream.
3. Two critical factors affect traffic smoothness and fuel economy of the mixed platoon. One is the average speed and the other is the market penetration of automated vehicle technology (using PnG strategy). The fuel-saving region becomes narrower, but fuel benefit becomes larger, as the market penetration increases.

ACKNOWLEDGMENTS

The research is supported by NSF China with grant 51205228. The authors highly appreciate Mr. Martin Kramer from RWTH Aachen University for his earlier work in building the traffic model.

REFERENCES

Adeli, H. & Ghosh-Dastidar, S. (2004), Mesoscopic-wavelet freeway work zone flow and congestion feature extraction model, *Journal of Transportation Engineering*, **130**(1), 94–103.

Adeli, H. & Jiang, X. (2009), *Intelligent Infrastructure: Neural Networks*, *Wavelets, and Chaos Theory for Intelligent Transportation Systems and Smart Structures*, CRC Press, Boca Raton, FL.

Adeli, H. & Samant, A. (2000), An adaptive conjugate gradient neural network—wavelet model for traffic incident detection, *Computer-Aided Civil and Infrastructure Engineering*, **15**(4), 251–60.

Beusen, B., Broekx, S., Denys, T., Beckx, C., Degraeuwe, B., Gijsbers, M., Scheepers, K., Govaerts, L., Torfs, R. & Int Panis, L. (2009), Using on-board logging devices to study the longer-term impact of an eco-driving course, *Transportation Research: Part D: Transport and Environment*, **14**(7), 514–20.

Castillo, E., Calvino, A., Nogal, M. & Lo, H. K. (2014), On the probabilistic and physical consistency of traffic random variables and models, *Computer-Aided Civil and Infrastructure Engineering*, **29**(7), 496–517.

Davis, L. C. (2004), Effect of adaptive cruise control systems on traffic flow, *Physical Review E*, **69**(6), 1–10.

Davis, L. C. (2007), Effect of adaptive cruise control systems on mixed traffic flow near an on-ramp, *Physica A: Statistical Mechanics and Its Applications*, **379**(1), 274–90.

Darbha, S. & Rajagopal, R. (1999), Intelligent cruise control systems and traffic flow stability, *Transportation Research: Part C: Emerging Technologies*, **7**(6), 329–52.

Dharia, A. & Adeli, H. (2003), Neural network model for rapid forecasting of freeway link travel time, *Engineering Applications of Artificial Intelligence*, **16**(7-8), 607–13.

Domínguez, R., Alonso, J., Onieva, E. & Gonzalez, C. (2013), A transferable belief model applied to lidar perception for autonomous vehicles, *Integrated Computer-Aided Engineering*, **20**(3), 289–302.

Ghosh-Dastidar, S. & Adeli, H. (2006), Neural network-wavelet micro-simulation model for delay and queue length estimation at freeway work zones, *Journal of Transportation Systems Engineering*, **132**(4), 331–41.

Helbing, D., Treiber, M., Kesting, A. & Schonhof, M. (2009), Theoretical vs. empirical classification and prediction of congested traffic states, *European Physical Journal B*, **69**, 583–98.

Hellström, E., Ivarsson, M., Aslund, J. & Nielsen, L. (2009), Look-ahead control for heavy trucks to minimize trip time and fuel consumption, *Control Engineering Practice*, **17**(2), 245–54.

Jerath, K. & Brennan, S. (2010), Adaptive cruise control: towards higher traffic flows, at the cost of increased susceptibility to congestion, in *Proceedings of AVEC,* Vol. **10**, Loughborough, UK.

Jiang, X. & Adeli, H. (2004), Wavelet packet-autocorrelation function method for traffic flow pattern analysis, *Computer-Aided Civil and Infrastructure Engineering*, **19**(6), 324–37.

Jiang, X. & Adeli, H. (2005), Dynamic wavelet neural network model for traffic flow forecasting, *Journal of Transportation Systems Engineering*, **131**(10), 771–9.

Kesting, A. & Treiber, M. (2008), How reaction time, update time, and adaptation time influence the stability of traffic flow, *Computer-Aided Civil and Infrastructure Engineering*, **23**(2), 125–37.

Kesting, A., Treiber, M. & Helbing, D. (2010), Enhanced intelligent driver model to access the impact of driving strategies on traffic capacity, *Philosophical Transactions of the Royal Society A: Mathematical, Physical and Engineering Sciences*, **368**, 4585–605.

Kobayashi, S., Plotkin, S. & Ribeiro, K. (2009), Energy efficiency technologies for road vehicles, *Energy Efficiency*, **2**(2), 125–37.

Li, S., Li, K., Rajamani, R. & Wang, J. (2011), Model predictive multi-objective vehicular adaptive cruise control, *IEEE Transactions on Control Systems Technology*, **19**(3), 556–66.

Li S., E., Peng, H., Li, K. & Wang, J. (2012), Minimum fuel control strategy in automated car-following scenarios, *IEEE Transactions on Vehicular Technology*, **61**(3), 998–1007.

Li S., E. & Peng, H. (2012), Strategies to minimize the fuel consumption of passenger cars during car-following scenarios, *Journal of Automobile Engineering*, **226**(3), 419–29.

Manzie, C., Watson, H. & Halgamuge, S. (2007), Fuel economy improvements for urban driving: hybrid vs. intelligent vehicles, *Transportation Research Part C: Emerging Technologies*, **15**(1), 1–16.

Ngoduy, D. & Wilson, R. E. (2014), Multi-anticipative nonlocal macroscopic traffic model, *Computer-Aided Civil and Infrastructure Engineering*, **29**(4), 248–63.

Setlur, P., Wagner, J., Dawson, D. & Samuels, B. (2003), Nonlinear control of a continuously variable transmission (CVT), *IEEE Transactions on Control Systems Technology*, **11**(1), 101–8.

Treiber, M., Hennecke, A. & Helbing, D. (2000), Congested traffic states in empirical observations and microscopic simulations, *Physical Review E*, **62**(2), 1805, DOI: http://dx.doi.org/10.1103/PhysRevE.62.1805.

Van Mierlo, J., Maggetto, G., Van de Burgwal, E. & Gense, R. (2004), Driving style and traffic measures-influence on vehicle emissions and fuel consumption, *Journal of Automobile Engineering*, **218**(1), 43–50.

Ward, J. & Wilson, R. (2011), Criteria for convective versus absolute string instability in car-following models. *Philosophical Transactions of the Royal Society A: Mathematical, Physical and Engineering Sciences*, **467**, 2185–208.

Wilson, R. (2008), Mechanisms for spatio-temporal pattern formation in highway traffic models, *Philosophical Transactions: Mathematical, Physical and Engineering Sciences*, **366**(1872), 2017–32.

Zarkadoula, M., Zoidis, G. & Tritopoulou, E. (2007), Training urban bus drivers to promote smart driving: a note on a Greek eco-driving pilot program, *Transportation Research Part D: Transport and Environment*, **12**(6), 449–51.

Zhang, J. & Ioannou, P. (2004), Longitudinal control of heavy trucks: environmental and fuel economy considerations, in *Intelligent Transportation Systems, 2004. Proceedings of the 7th International IEEE Conference*, pp. 761–66.

NOTATIONS

Symbol	*Description*	*Unit*
α_{thr}	Throttle angle	%
δ	Acceleration exponent (IDM)	–
η_T	Mechanical efficiency of the driveline	–
ξ_{min}, ξ_{max}	Bounds for distance error	m
τ_b	Time constant of braking dynamics	sec
τ_h	Time headway (IDM, PnG)	sec
ω_e	Engine speed	rad/s
$\omega_{emin}, \omega_{emax}$	Bounds of engine speed	rad/s
Δv	Relative speed to the front vehicle	m/s
ΔF	Force demand on wheels	N
Δd	Distance error	m
$\Theta_a, \Theta_s, \Theta_d, \Theta_{\Delta v}$	Conditions to activate the braking controller (PnG)	–
a	Vehicle acceleration	m/s^2
a_0	Comfortable acceleration (IDM)	m/s^2
a_{des}	Desired acceleration	m/s^2
b_0	Comfortable deceleration (IDM)	m/s^2
d	Inter-vehicle distance	m
d_0	Minimum gap (IDM)	m
d_{des}	Desired inter-vehicle distance	m
i_g	Speed ratio of automatic transmission	–
f	Coefficient of rolling resistance	–
g	Constant of gravity	m/s^2
q_s	Static fueling rate	g/s
n	Control step in PnG	–
k	Index of vehicle in a platoon	–
k_e	Correction coefficient for transient fuel	–
v	Vehicle speed	m/s
v_0	Desired speed (IDM)	m/s
r_w	Wheel radius	m
C_A	Coefficient of aerodynamic drag	kg/m
$C_b(\cdot)$	Braking control law (PnG)	–
K_b	Braking gain	N.m/MPa
M	Vehicle mass	kg
P_{brk}	Brake pressure	MPa
Q_s	Engine fuel consumption rate	g/s
T_f	Final time in optimal control	sec
T_b	Brake torque	N.m
T_e	Engine torque	N.m
T_{emin}, T_{emax}	Bounds of engine torque	N.m
T_{eBSFC}	Engine torque at BSFC point	N.m